Atmospheric Opacity in the Schumann-Runge Bands and the Aeronomic Dissociation of Water Vapor

J. E. FREDERICK AND R. D. HUDSON

Laboratory for Planetary Atmospheres, NASA/Goddard Space Flight Center, Greenbelt, MD 20771

(Manuscript received 30 October 1979, in final form 15 January 1980)

ABSTRACT

Knowledge of the aeronomic production of odd hydrogen in the dissociation of water vapor is limited by uncertainties in the penetration of solar irradiance in the Schumann-Runge bands of O_2 and by incomplete information concerning the products of photolysis at Lyman alpha. Consideration of all error sources involved in computing the H_2O dissociation rate in the wavelength region 175–200 nm leads to an estimated uncertainty of ±35% at an altitude of 90 km for an overhead sun. The uncertainty increases with decreasing altitude such that the true dissociation rate at 60 km for an overhead sun lies between 0.45 and 1.55 times the result computed using the best input parameters currently available. Calculations of the H_2O dissociation rate by Lyman alpha should include the variation in O_2 opacity across the solar line width. Neglect of this can lead to errors as large as 50% at altitudes where the process is the major source of odd hydrogen.

1. Introduction

The aeronomic dissociation of water vapor below 100 km in altitude occurs at Lyman alpha (121.56 nm) and in the spectral region of the Schumann-Runge (SR) bands (175–200 nm) where absorption by O_2 controls the penetration of the required solar irradiance. This paper examines the atmospheric attenuation of solar photons in the SR bands and presents values of the H_2O dissociation rate appropriate for use in photochemical models. Although a number of studies of these topics have been reported (Kockarts, 1971; Anderson, 1971; Park, 1974; Blake, 1979), they have not explicitly addressed the uncertainties encountered. A major goal of the present work is to assess the likely error involved in calculations of the odd hydrogen production rate in the upper stratosphere, mesosphere and lower thermosphere. The need for this study arises from discrepancies which seem to exist in reconciling theoretical predictions with available odd oxygen measurements in the uppermost stratosphere and mesosphere (Riegler *et al.*, 1977; Wofsy, 1978; Frederick *et al.*, 1978a). The calculations reported here employ absorption cross sections for the O_2 SR bands computed from the oscillator strengths and rotational linewidths of Frederick and Hudson (1979, 1980). The error bars reported by these authors imply an uncertainty in the dissociation rate of H_2O which increases rapidly with decreasing altitude. We evaluate these errors in detail and also show that considerable uncertainty exists in computing the odd hydrogen production rate due to absorption of Lyman alpha radiation.

The chemical processes preceded by the dissociation of water vapor were first discussed by Bates and Nicolet (1950) as a means of explaining the presence of vibration-rotation bands of the hydroxyl radical in the nightglow as observed by Meinel (1950). Improved values of the incident solar irradiance and of relevant rate coefficients which later became available led to the realization that reactions involving odd hydrogen (H, OH, HO_2) were the principal loss mechanism for odd oxygen (O, O_3) in the uppermost stratosphere and throughout the mesosphere (Hunt, 1966). The major sources of odd hydrogen are the reaction

$$O(^1D) + H_2O \rightarrow OH + OH[k_1] \qquad (R1)$$

and the photodissociation of water vapor. The odd hydrogen so formed destroys odd oxygen in a catalytic cycle whose rate limiting step is

$$OH + O(^3P) \rightarrow H + O_2. \qquad (R2)$$

Photodissociation becomes more important than reaction (R1) in the lower mesosphere and dominates at higher altitudes.

The possible paths for water vapor photodissociation are

$$H_2O + h\nu \rightarrow H_2 + O(^3P) \quad (\lambda < 247.5 \text{ nm}), \qquad (R3a)$$

$$\rightarrow OH + H \quad (\lambda < 242.6 \text{ nm}), \qquad (R3b)$$

$$\rightarrow H_2 + O(^1D) \quad (\lambda < 177.6 \text{ nm}), \qquad (R3c)$$

$$\rightarrow H + H + O(^3P) \quad (\lambda < 130.8 \text{ nm}). \qquad (R3d)$$

Although path (a) requires the smallest energy, the transition is spin-forbidden and apparently does not occur to a measurable extent. All available data indicate that path (b) dominates at most wavelengths; however, as discussed below, there are theoretical reasons for believing that branch (c) may be significant when Lyman alpha radiation is involved. Branch (R3d) apparently does not occur. McNesby *et al.* (1962) studied the products of H_2O dissociation using the 123.6 nm krypton resonance line as a light source. They found that 25% of the dissociations proceeded by branch (R3c). Using a broad-band excitation source, Stief *et al.* (1975) found (R3c) to occur in 11% of the dissociations for the wavelength range 105–145 nm. The value dropped to <1% for λ = 145–185 nm. A continuum light source as used by Stief *et al.* (1975) excites numerous upper states only some of which predissociate via branch (R3c); hence, the results do not necessarily give the products of dissociation at Lyman alpha. Qualitative arguments presented by Herzberg (1966) show that the products H_2 + O(^{1}D) are most probable if the upper electronic state involved in the transition is excited into a bending mode, (ν_1,ν_2,ν_3) = (0, 1, 0). Under such circumstances the distance between the hydrogen atoms is reduced and the formation of a bond to give H_2 is more probable than in a (0, 0, 0) state.

Bell (1965) has performed vibrational analyses of several H_2O bands in the vicinity of Lyman alpha. The 123.6 nm krypton line used by McNesby *et al.* (1962) falls in Bell's α_1 system with a band head at 124.063 nm and corresponds to the (0, 0, 0) ← (0, 0, 0) transition between the ground and excited electronic states. Yet even in this case, where no bending mode is involved, one-fourth of the dissociations appear to give H_2 + O(^{1}D). Two bands overlap at Lyman alpha, one being the β_2 system corresponding to (0, 0, 0) ← (0, 0, 0) where the upper electronic state differs from that in the α system. The second system, identified by Bell (1965) as α_2, has the upper state in a bending mode (0, 1, 0) ← (0, 0, 0). By the arguments of Herzberg (1966), the products H_2 + O(^{1}D) are more likely in the predissociation of the α_2 band system than in α_1 where the results of McNesby *et al.* (1962) apply. Hence, no laboratory measurement reported to data can definitively fix the branching ratio among the various paths when Lyman alpha is the source, either because the data were not taken in the appropriate band system or because the spectral interval covered in the experiment was too large to be applied to the atmospheric dissociation. The presence of hydroxyl radical emissions in the nightglow is evidence that (R3b) indeed occurs in the 80–90 km altitude region where Lyman alpha dominates H_2O photodissociation. However, the need to include poorly known parameters to describe transport processes in calculations allows a wide range of observed nightglow intensities to be fit (Frederick *et al.*, 1978b); thus, agreement between model results and measurement cannot firmly establish the importance of the various dissociation paths at Lyman alpha.

2. Dissociation of H_2O in the Schumann-Runge bands

Rotational line structure in the O_2 cross section greatly complicates a calculation of the 175–200 nm solar irradiance reaching a given level in the atmosphere. In computing the H_2O dissociation rate it is acceptable to adopt constant values of the incident solar irradiance and of the H_2O cross section in wavenumber intervals of width 500 cm^{-1}. The dissociation rate of water vapor in the O_2 Schumann-Runge band region is then

$$J(H_2O) = \sum_i \sigma_i(H_2O)\phi(i)e^{-\tau_i(O_3)}\bar{T}_i(N), \qquad (1)$$

where i labels a 500 cm^{-1} interval, σ_i is the average H_2O cross section, $\phi(i)$ the integrated solar irradiance (photons cm^{-2} s^{-1}), and $\tau_i(O_3)$ the slant path optical depth due to ozone, which is small above 50 km. The transmission function is defined by

$$\bar{T}_i(N) = \frac{1}{\Delta\lambda_i}\int_{\lambda_i}^{\lambda_i+\Delta\lambda_i} d\lambda \times \exp\left\{-\int_{z(N)}^{\infty} dz'\sigma_\lambda(O_2; z')[O_2(z')]\sec\theta\right\}, \qquad (2)$$

where N, the O_2 column density, is the most meaningful vertical coordinate, $\Delta\lambda_i$ the width of the spectral interval, $\sigma_\lambda(O_2; z)$ the O_2 cross section at altitude $z = z(N)$ and θ the solar zenith angle. The O_2 cross section is temperature dependent (Frederick and Hudson, 1980) and must therefore be included in the integral over altitude. A contribution from the continuum which underlies the SR bands, as tabulated by Hudson and Mahle (1972), is included in $\sigma_\lambda(O_2; z)$. Frederick and Hudson (1979, 1980) have discussed the derivation of the molecular parameters required to compute $\sigma_\lambda(O_2; z)$ and details of the numerical model used so that no further discussion need be given here.

The spectral region from 48 600 to 57 000 cm^{-1} was divided into 17 pieces of width 500 cm^{-1} (except for the first interval which extended from 48 600 to 49 000 cm^{-1}) and the transmission function in each was computed using the density and temperature profiles of the *U.S. Standard Atmosphere 1976*. Within each 500 cm^{-1} interval the cross section was calculated on a wavenumber grid which resolved all rotational structure. In practice the slant path O_2 column density, $N\sec\theta$, is an acceptable vertical coordinate since the variation of $\bar{T}_i$ with temperature is not great in the range encountered over one to two atmospheric scale heights. Fig. 1 presents values

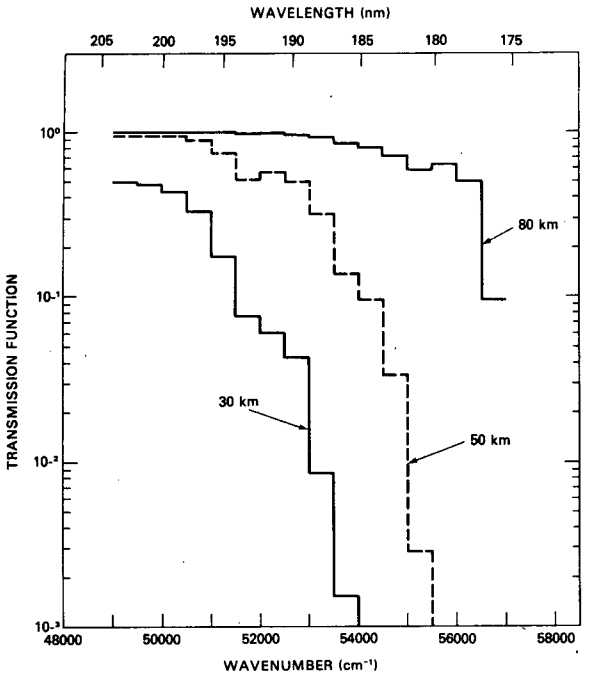

FIG. 1. Transmission of solar photons in the Schumann-Runge bands to various altitudes for an overhead sun. Values refer to intervals of width 500 cm^{-1}.

of the $\tilde{T}_i$, $i = 1, 17$, at 80, 50 and 30 km, for an overhead sun and the complete set of transmission functions appears in the Appendix. Wavelengths < 177 nm are absorbed primarily above the mesopause with a transmission at 80 km of 10% or below. Less than 10% of the photons at wavelengths below 185 and 194 nm reach the stratopause and 30 km, respectively. We note that the O_2 rotational line widths used in our study tend to be smaller than those employed in past calculations while the band oscillator strengths are roughly the same (Kockarts, 1971; Blake, 1979). Detailed discussion of the differences appears in Frederick and Hudson (1979, 1980). In the wings of an absorption line the cross section is proportional to the product of the oscillator strength and linewidth. At low altitudes solar radiation penetrates primarily in the line wings where the new cross sections are smaller than believed previously.

The error bars on the oscillator strengths and linewidths lead to uncertainties in the transmission functions which increase with decreasing altitude roughly as the O_2 column content. To study this effect in detail we have computed three sets of cross sections for the SR bands based on the best estimate of oscillator strengths and linewidths and on the upper and lower limits defined by the error bars of Frederick and Hudson (1979). Fig. 2 presents ratios of transmission functions based on the upper and lower limits of the O_2 cross section to those computed with the best estimates. Results for the three intervals shown, 51 000–51 500, 53 000–53 500 and 55 500–56 000 cm^{-1}, are representative of those for all other SR band regions. At small O_2 column contents the errors are negligible but increase exponentially as one proceeds deeper into the atmosphere. For example, in the interval 55 500–56 000 cm^{-1}

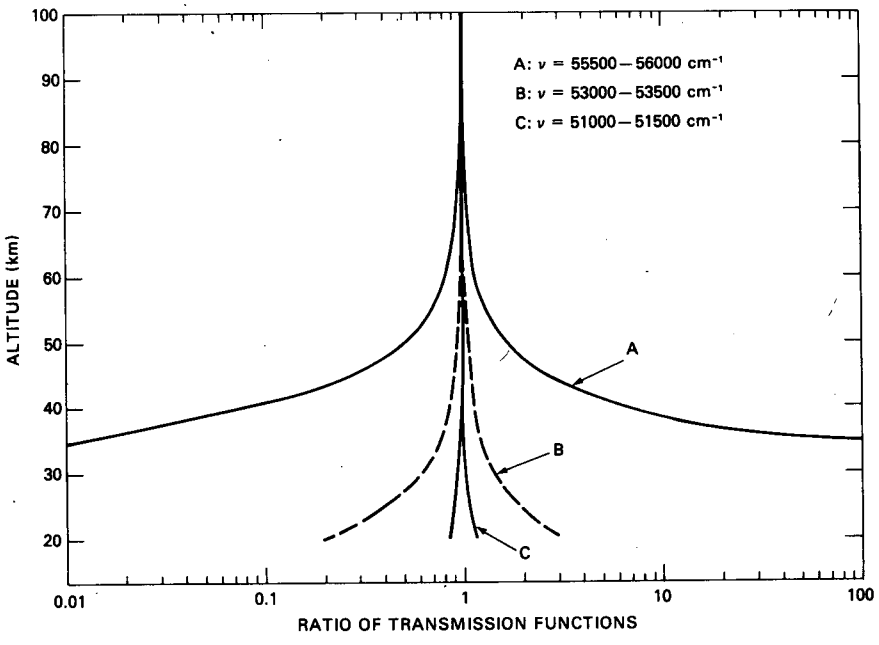

FIG. 2. Ratios of transmission functions computed with upper and lower limits of the O_2 cross section to those based on the best estimates. Values refer to an overhead sun.

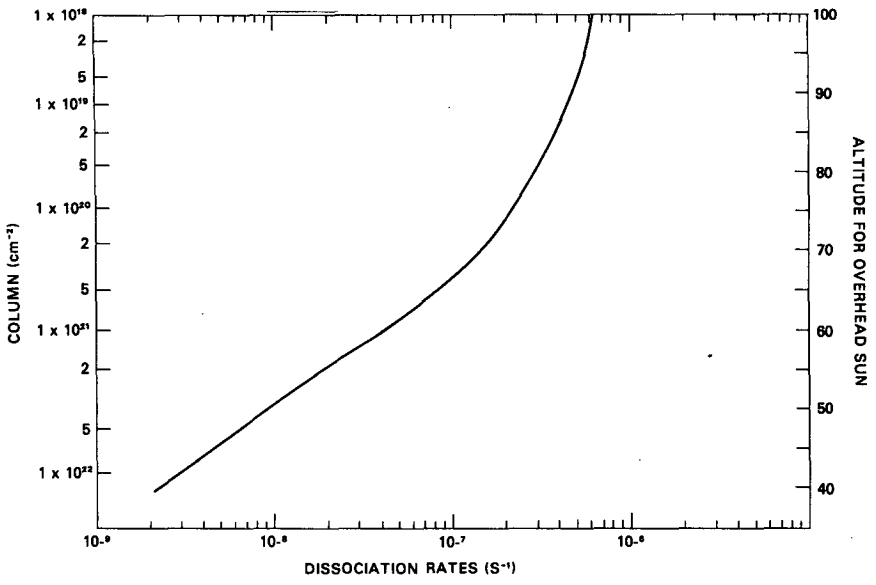

FIG. 3. Dissociation rate of H_2O in the spectral region of the O_2 Schumann-Runge bands. The O_2 column density measured along the solar beam is the physically relevant vertical coordinate.

(180.18–178.57 nm) the true number of photons which reach 50 km in altitude for an overhead sun may lie anywhere between 0.5 and 1.6 times that predicted from the best estimate parameters of Frederick and Hudson (1979). At smaller wavenumbers the uncertainties are much less. In the interval 51 000–51 500 cm^{-1} (196.08–194.17 nm) the overhead sun transmission is known to better than ±1% due to the small O_2 opacity. If one were interested only in the total number of photons which penetrate in the SR bands, even the greatest uncertainty given above would not be highly significant since at a given altitude most photons lie in optically thin bands. Thus, errors in the cross section have a minor effect on transmission. In the case of water vapor dissociation, however, the H_2O cross section decreases by a factor of nearly 5×10^4 between 175 and 200 nm so that errors in O_2 opacity at short wavelengths directly affect the destruction rate.

Calculations of the water vapor dissociation rate between 175 and 200 nm here use the solar irradiance data of Brueckner *et al.* (1976) and the H_2O cross sections of Watanabe and Zelikoff (1953). In our early trials we used the high-resolution solar irradiance measurements from which the 0.5 nm integrated data of Brueckner *et al.* (1976) were derived. However, we found that inclusion of the detailed solar irradiance altered the results by only a fraction of a percent while increasing computing time significantly. We estimate the uncertainty in the input data to be ±20% for the irradiance and ±15% for the H_2O cross section based on discussions in the original papers and by Hudson (1971). Ozone opacity is included using the profile of Krueger and Minzner (1976) and cross sections compiled by Ackerman (1971).

Fig. 3 and Table 1 present the H_2O dissociation rate in the SR band region as a function of O_2 column density. For use in photochemical calculations interpolation between the values of Table 1 should use O_2 column density along the solar beam path as the vertical coordinate. The tabulated results are

TABLE 1. Dissociation rate of water vapor in the spectral region of the Schumann-Runge bands.

Column O_2 (cm^{-2})	z_0** (km)	Dissociation*** rate (s^{-1})
3.922 + 16*	120	6.79 − 7
7.262 + 16	115	6.75 − 7
1.555 + 17	110	6.69 − 7
3.901 + 17	105	6.53 − 7
1.060 + 18	100	6.17 − 7
2.905 + 18	95	5.54 − 7
7.718 + 18	90	4.69 − 7
1.960 + 19	85	3.75 − 7
4.716 + 19	80	2.87 − 7
1.078 + 20	75	2.10 − 7
2.358 + 20	70	1.41 − 7
4.939 + 20	65	8.35 − 8
9.919 + 20	60	4.17 − 8
1.919 + 21	55	1.86 − 8
3.607 + 21	50	8.77 − 9
6.756 + 21	45	4.47 − 9
1.299 + 22	40	2.27 − 9

* Read 3.922 + 16 as 3.922×10^{16}.

** Altitude corresponding to the given O_2 column for an overhead sun.

*** Reported values include ozone attenuation based on the profile of Krueger and Minzner (1976). See text for discussion.

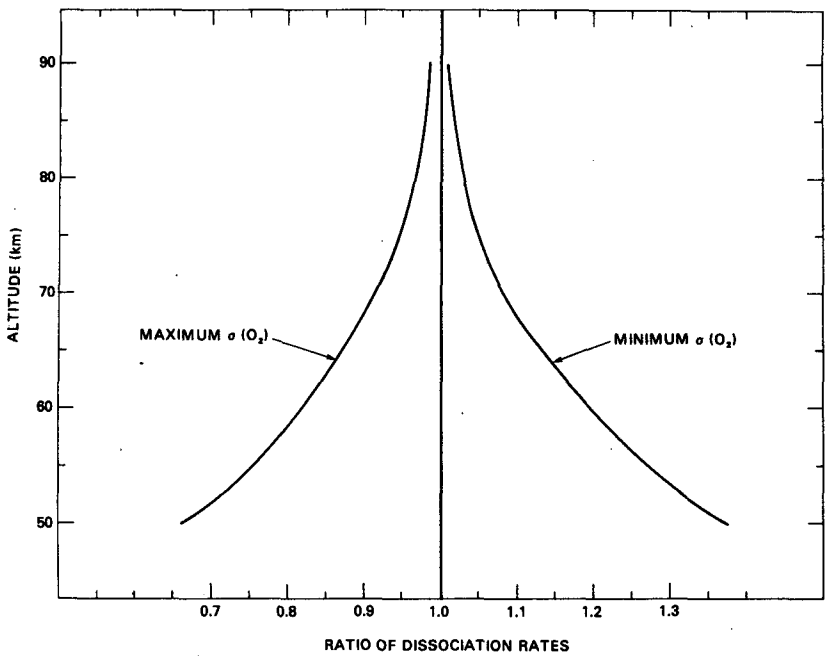

FIG. 4. Uncertainty in the H_2O dissociation rate for an overhead sun due to possible errors in the O_2 opacity. The abscissa gives the ratio of the H_2O dissociation rates computed with upper and lower limits of the O_2 cross section to rates based on the best estimates.

then sufficient to define the dissociation rate over a range of solar zenith angle. Since the tabulated results were computed for a particular temperature distribution and an overhead sun, use of the values at solar zenith angles > 70–$75°$ will introduce a small error due to the temperature dependence in the cross section. In practice, this is not a major limitation. As discussed later, attenuation by O_3 is small at altitudes where dissociation in the SR bands is significant. Hence, use of the results of Table 1, which include a specific ozone model, is not highly restrictive. The uncertainties in the dissociation rate due to error bars on the O_2 cross section appear in Fig. 4. For an overhead sun the uncertainty spread is approximately ± 10, ± 20 and $\pm 30\%$ at 68, 58 and 52 km, respectively. Although the potential error continues to increase toward lower altitudes, photodissociation becomes a small source of odd hydrogen compared to reaction (R1).

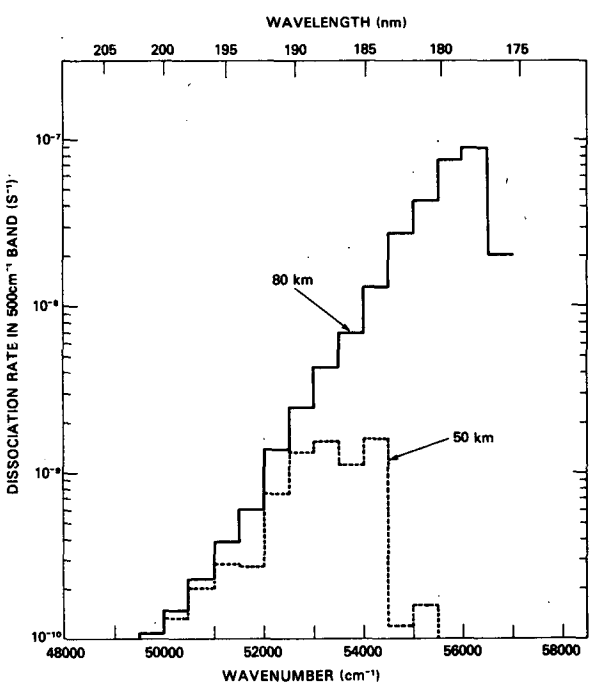

FIG. 5. Contributions to the H_2O dissociation rate from 175 to 200 nm in 500 cm^{-1} bands for an overhead sun.

Fig. 5 presents the H_2O dissociation rate in 500 cm^{-1} intervals for altitudes of 80 and 50 km with an overhead sun. At the mesopause most of the dissociation occurs at the shortest wavelengths (175–184 nm) where the H_2O cross section is large. Near the stratopause, however, the optical depth is sufficiently great that H_2O dissociation occurs at longer wavelengths, 184–195 nm, despite the small cross section in this region.

3. Dissociation at Lyman alpha

Aeronomic models have generally computed the H_2O dissociation rate due to the Lyman alpha line by adopting single values for the O_2 and H_2O cross sections and the integrated solar irradiance as tabu-

lated, for example, by Ackerman (1971). This is an oversimplification for the following reasons: The absorption cross section of water vapor at wavelengths near Lyman alpha consists of bands whose finestructure has not been resolved in the laboratory and the value reported by Watanabe and Zelikoff (1953) represents an average over a 0.1 nm instrument bandpass. The major point here is that the solar irradiance varies by roughly a factor of 2 over a 0.1 nm interval about the line center. Hence, the value of the unattenuated dissociation rate depends on the distribution of water vapor lines over the solar Lyman alpha profile. Although no laboratory data are available for the line positions, calculations presented below based on various extreme assumptions show that the H_2O dissociation rate is rather sensitive to this input. In addition, the O_2 absorption cross section in the vicinity of Lyman alpha consists of band systems whose rotational structure has not been resolved (Hudson, 1971) and the Lyman alpha line falls in a minimum between two bands. Ogawa (1968) has examined the O_2 absorption cross section with a resolution of 2–3 $\times 10^{-3}$ nm and found a variation of 0.96–0.97 $\times 10^{-20}$ cm^2 to 2.1 $\times 10^{-20}$ cm^2 over a wavelength range of $\pm$0.05 nm about the Lyman alpha line center. The absolute values of the cross section including the smearing effect of the instrument are estimated here as accurate to $\pm$10% in view of the overall good agreement among the lower resolution results of various investigators as reviewed by Hudson (1971). Values are generally in the range 1.00 $\times 10^{-20}$ to 1.08 $\times 10^{-20}$ cm^2 although it is clear from the results of Ogawa (1968) that the result obtained depends on instrument bandwidth. The above point would not pose a problem were it not for the variation of the water vapor absorption cross section and solar irradiance across the linewidth. The solar line displays a well-known reversal due to absorption by exospheric hydrogen with the irradiance at line center being roughly one-half of the peak values on either side (Bruner and Rense, 1969; Meier and Prinz, 1970; Vidal-Madjar *et al.*, 1973). The total Lyman alpha energy which reaches a given altitude depends on the product of an incident irradiance which changes appreciably across the linewidth and a wavelength-dependent attenuation factor. The result of a detailed treatment of this Lyman alpha attenuation, as given below, differs significantly from that predicted using single values for the irradiance and O_2 cross section.

Table 2 presents the best estimates of the H_2O dissociation rate due to Lyman alpha radiation. The calculation was performed by dividing the spectral region from 0.10 nm below to 0.09 nm above line center into 76 intervals each of which was assigned by O_2 cross-section value taken from the results of Ogawa (1968) and a solar irradiance based on the profile shape of Meier and Prinz (1970) normalized to the integrated value 3.0 $\times 10^{11}$ photons cm^{-2} s^{-1} (Ackerman, 1971). Fig. 6 presents the cross sections and shape of the solar line. The H_2O cross section was assumed to have no rotational structure with the values 1.32 $\times 10^{-17}$ and 1.56 $\times 10^{-17}$ cm^2 for the spectral regions less than 0.05 nm and more than 0.05 nm from line center, respectively. These, with the value 1.44 $\times 10^{-17}$ cm^2 at the core of the line, are consistent with the data of Watanabe and Zelikoff (1953). In using the values of Table 2 the O_2 column density, as opposed to altitude, is the physically meaningful vertical coordinate. To test the effect of a variable O_2 cross section across the solar line we have computed the H_2O dissociation rate using the constant values $\sigma(O_2) = 1.00 \times 10^{-20}$ and 1.08 $\times 10^{-20}$ cm^2. Comparison of these results with the best estimates of Table 2 for an overhead sun yields the ratios shown in Fig. 7. At 70 km Lyman alpha is the major contributor to H_2O dissociation, yet results based on single values of the O_2 cross section as reported in the literature are 25–51% larger than predicted by the more complete calculation. At high altitudes the average O_2 cross section weighted by the photon distribution across the Lyman alpha profile is larger than 1.08 $\times 10^{-20}$ cm^2 due to the increase in $\sigma(O_2)$ toward wavelengths smaller than that of line center. The detailed calculation therefore gives dissociation rates smaller than the simplified cases. At lower altitudes photons which lie shortward of line center are strongly depleted, leaving the long wavelength lobe of the profile to experience an average cross section $< 1.00 \times 10^{-20}$ cm^2. Hence, the detailed calculation here produces a dissociation rate larger than either case with constant $\sigma(O_2)$.

TABLE 2. Dissociation rate of water vapor due to Lyman alpha.

Column O_2 (cm^{-2})	z_0** (km)	J_α (H_2O) (s^{-1})
3.922 + 16*	120	4.32 − 6
7.262 + 16	115	4.31 − 6
1.555 + 17	110	4.30 − 6
3.901 + 17	105	4.28 − 6
1.060 + 18	100	4.24 − 6
2.905 + 18	95	4.14 − 6
7.718 + 18	90	3.87 − 6
1.960 + 19	85	3.30 − 6
4.716 + 19	80	2.31 − 6
1.078 + 20	75	1.11 − 6
2.358 + 20	70	2.70 − 7
4.939 + 20	65	1.90 − 8
9.919 + 20	60	1.38 − 10
1.919 + 21	55	1.66 − 14
3.607 + 21	50	1.39 − 21

* Read 3.922 + 16 as 3.922 $\times 10^{16}$.

** Altitude corresponding to the given O_2 column density for an overhead sun.

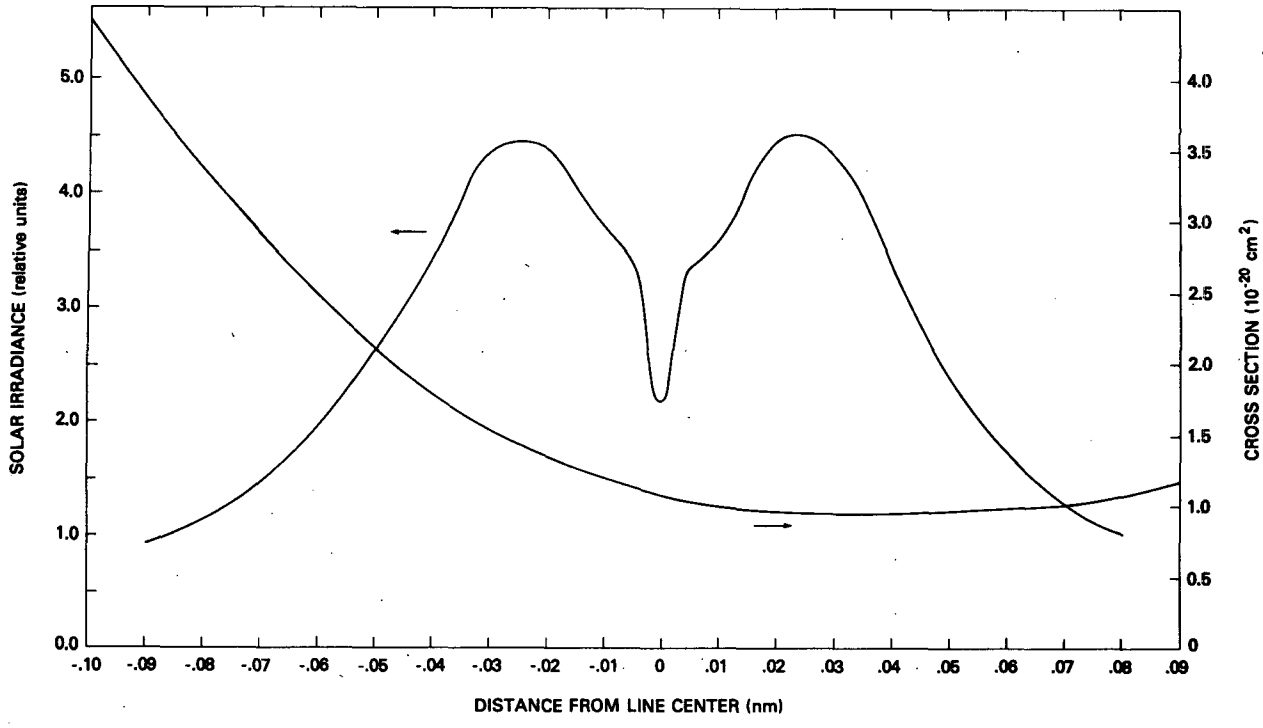

FIG. 6. Profile of the unattenuated Lyman alpha line and of the O_2 cross section in the vicinity of 1215.6 nm.

The maximum possible influence of rotational structure in the H_2O cross section on the dissociation rate at Lyman alpha is easily evaluated. The experimental constraint imposed by the data of Watanabe and Zelikoff (1953) requires the average cross section over a ± 0.05 nm interval centered on

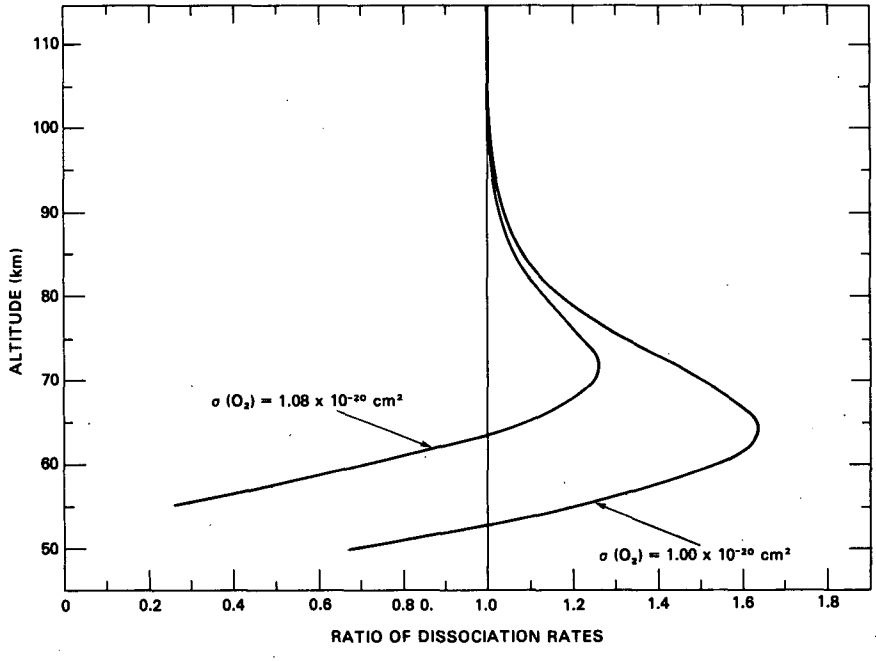

FIG. 7. Errors in the H_2O dissociation rate by Lyman alpha due to the adoption of a constant O_2 cross section. Reported values are the ratios of rates computed with constant O_2 cross sections to those based on the variable cross section of Fig. 6. The sun is overhead.

Lyman alpha to be

$$\frac{1}{2\Delta\lambda}\int_{\lambda_0-\Delta\lambda}^{\lambda_0+\Delta\lambda} d\lambda\sigma_\lambda(H_2O) = 1.44 \times 10^{-17}\ \text{cm}^2, \quad (2)$$

where $\Delta\lambda = 0.055$ nm and $\lambda_0 = 121.56$ nm. For simplicity the instrument response function has been assumed rectangular. The measured cross section shows no rotational structure which implies that the spacing between successive lines is much less than the instrument bandpass. However, to establish extreme limits on the dissociation rate we assume that the cross section in the ± 0.05 nm band about line center is concentrated entirely in a square wave of width 0.025 nm. Outside this band we adopt average cross sections of 1.32×10^{-17} and 1.56×10^{-17} cm^2 for wavelengths less than 121.51 nm and greater than 121.61 nm, respectively. These values are consistent with the results of Watanabe and Zelikoff (1953). If the single line is placed at the center of Lyman alpha where the irradiance is a minimum, an unattenuated dissociation rate of $J(\text{Ly}\alpha) = 3.00 \times 10^{-6}$ s^{-1} results. If the cross section is displaced 0.024 nm to the long wavelength side of line center the dissociation rate becomes 5.04×10^{-6} s^{-1}. This compares to the best estimate in Table 2 of 4.32×10^{-6} s^{-1}. Thus, the error introduced in the unattenuated water vapor dissociation rate at Lyman alpha due to the neglect of rotational structure must be between -31 and $+17\%$ of the tabulated result.

4. Comparison of photodissociation and chemical production

Figs. 8a and 8b compare the H_2O dissociation rates due to Lyman alpha, the spectral region of the SR bands, solar photons of wavelength < 175 nm except Lyman alpha, and reaction (R1). Wavelengths longer than 205 nm make a negligible contribution to dissociation. The O(^{1}D) profile required in evaluating the rate of (R1) is based on the Krueger and Minzner (1976) ozone model, the solar irradiance of Nicolet (1975) and quenching rates reported by Streit *et al.* (1976). For wavelengths < 175 nm the solar irradiance data of Heroux and Swirbalus (1976) multiplied by 1.1 were used. This correction makes these data agree with the results of Brueckner *et al.* (1976) between 175 and 210 nm. For an overhead sun Lyman alpha absorption is the major mechanism for dissociating H_2O above 68 km, the SR band region dominates between 61 and 68 km only, with (R1) supplying the major odd hydrogen source at lower altitudes. As the solar zenith angle increases, dissociation in the SR bands becomes relatively more important. For an 85° sun the SR band dissociation dominates between 71 and 83 km. The best estimate for the O_2 cross section predicts an H_2O dissociation rate between 175 and 200 nm that is 10% or more to the O(^{1}D) + H_2O source down to 52 km for an overhead sun and down to 62 km for a solar zenith angle of 85°.

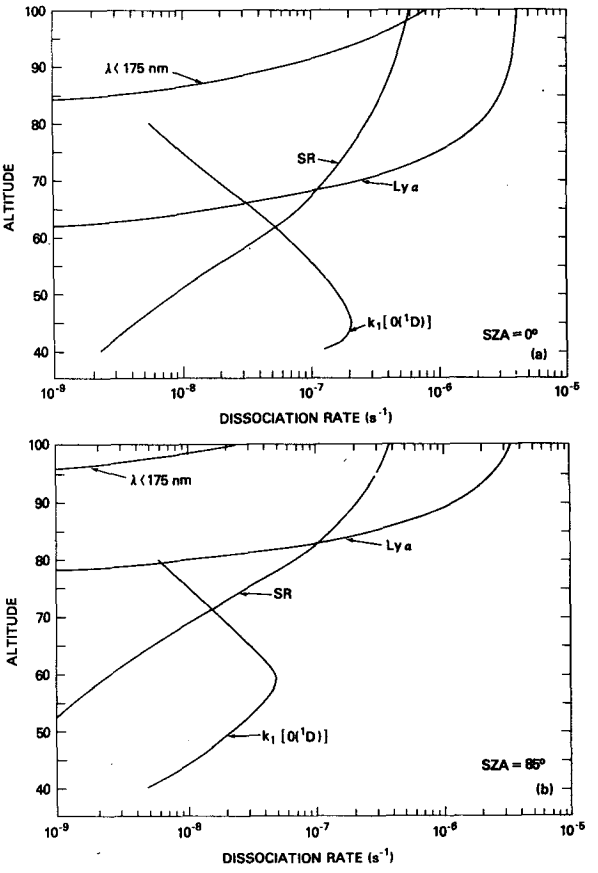

FIG. 8. Comparison of water vapor destruction rates by photodissociation and chemical paths for solar zenith angles of 0° (a) and 85° (b).

5. Conclusions

Potential sources of error involved in computing the odd hydrogen production rate above 50 km are due to uncertainties in the products of H_2O dissociation by Lyman alpha and the spread in values of O_2 absorption cross sections in the Schumann-Runge bands allowed by the available data. Calculations of the H_2O dissociation rate due to Lyman alpha should include the variation of the O_2 cross section across the solar line width. The more detailed treatment yields results which are as much as 50% larger than when one adopts a constant O_2 cross section. Present uncertainties in the H_2O cross section and solar irradiance imply that the true unattenuated dissociation rate in the Schumann-Runge region, 175–200 nm, lies between 0.65 and 1.35 times the best estimates. Potential errors in the O_2 cross sections lead to an additional uncertainty which is altitude dependent. For an overhead sun these expand the error limits such that at 60 km for an overhead sun

the actual rate may lie anywhere between 0.45 and 1.55 times the computed value.

APPENDIX

Tabulation of Atmospheric Transmission Functions in the Spectral Region of the O_2 Schumann-Runge Bands

TABLE A1. Spectral intervals for which transmission functions are computed.

Label (i)	Wavenumber range (cm^{-1})
1	48 600–49 000
2	49 000–49 500
3	49 500–50 000
4	50 000–50 500
5	50 500–51 000
6	51 000–51 500
7	51 500–52 000
8	52 000–52 500
9	52 500–53 000
10	53 000–53 500
11	53 500–54 000
12	54 000–54 500
13	54 500–55 000
14	55 000–55 500
15	55 500–56 000
16	56 000–56 500
17	56 500–57 000

TABLE A2. Transmission functions $\bar{T}$ for each spectral interval i.

z (km)*	N (cm^{-2})*	$\bar{T}$ (i = 1)	$\bar{T}$ (i = 2)
120	3.922 + 16**	9.998 − 1	9.998 − 1
115	7.262 + 16	9.998 − 1	9.998 − 1
110	1.555 + 17	9.998 − 1	9.998 − 1
105	3.901 + 17	9.998 − 1	9.998 − 1
100	1.060 + 18	9.998 − 1	9.998 − 1
95	2.905 + 18	9.998 − 1	9.998 − 1
90	7.718 + 18	9.997 − 1	9.997 − 1
85	1.960 + 19	9.996 − 1	9.996 − 1
80	4.716 + 19	9.991 − 1	9.991 − 1
75	1.078 + 20	9.986 − 1	9.984 − 1
70	2.358 + 20	9.969 − 1	9.968 − 1
65	4.939 + 20	9.938 − 1	9.936 − 1
60	9.919 + 20	9.879 − 1	9.872 − 1
55	1.919 + 21	9.767 − 1	9.755 − 1
50	3.607 + 21	9.568 − 1	9.543 − 1
45	6.756 + 21	9.207 − 1	9.160 − 1
40	1.299 + 22	8.534 − 1	8.452 − 1
35	2.595 + 22	7.288 − 1	7.156 − 1
30	5.382 + 22	5.193 − 1	5.007 − 1
25	1.145 + 23	2.483 − 1	2.303 − 1
20	2.480 + 23	4.902 − 1	4.182 − 2

z (km)	$\bar{T}$ (i = 3)	$\bar{T}$ (i = 4)	$\bar{T}$ (i = 5)
120	9.998 − 1	9.999 − 1	9.999 − 1
115	9.998 − 1	9.999 − 1	9.999 − 1
110	9.998 − 1	9.999 − 1	9.999 − 1
105	9.998 − 1	9.999 − 1	9.999 − 1
100	9.998 − 1	9.999 − 1	9.999 − 1
95	9.998 − 1	9.999 − 1	9.998 − 1
90	9.997 − 1	9.998 − 1	9.996 − 1
85	9.996 − 1	9.995 − 1	9.990 − 1

TABLE A2. (*Continued*)

z (km)	$\bar{T}$ (i = 3)	$\bar{T}$ (i = 4)	$\bar{T}$ (i = 5)
80	9.991 − 1	9.992 − 1	9.977 − 1
75	9.983 − 1	9.983 − 1	9.948 − 1
70	9.967 − 1	9.962 − 1	9.890 − 1
65	9.933 − 1	9.919 − 1	9.783 − 1
60	9.865 − 1	9.835 − 1	9.602 − 1
55	9.740 − 1	9.674 − 1	9.309 − 1
50	9.512 − 1	9.377 − 1	8.846 − 1
45	9.100 − 1	8.861 − 1	8.129 − 1
40	8.350 − 1	7.996 − 1	7.056 − 1
35	7.001 − 1	6.550 − 1	5.472 − 1
30	4.805 − 1	4.333 − 1	3.342 − 1
25	2.125 − 1	1.799 − 1	1.230 − 1
20	3.548 − 2	2.683 − 2	1.513 − 2

z (km)	$\bar{T}$ (i = 6)	$\bar{T}$ (i = 7)	$\bar{T}$ (i = 8)
120	1.000 + 0	1.000 + 0	9.999 − 1
115	1.000 + 0	9.999 − 1	9.999 − 1
110	1.000 + 0	9.999 − 1	9.999 − 1
105	9.999 − 1	9.998 − 1	9.997 − 1
100	9.998 − 1	9.994 − 1	9.994 − 1
95	9.996 − 1	9.984 − 1	9.984 − 1
90	9.988 − 1	9.958 − 1	9.961 − 1
85	9.971 − 1	9.895 − 1	9.906 − 1
80	9.932 − 1	9.757 − 1	9.789 − 1
75	9.848 − 1	9.483 − 1	9.568 − 1
70	9.683 − 1	9.007 − 1	9.217 − 1
65	9.391 − 1	8.308 − 1	8.704 − 1
60	8.931 − 1	7.420 − 1	7.981 − 1
55	8.283 − 1	6.370 − 1	6.994 − 1
50	7.423 − 1	5.179 − 1	5.732 − 1
45	6.333 − 1	3.942 − 1	4.330 − 1
40	5.007 − 1	2.766 − 1	2.947 − 1
35	3.443 − 1	1.686 − 1	1.649 − 1
30	1.785 − 1	7.627 − 2	6.089 − 2
25	5.173 − 2	1.815 − 2	9.626 − 3
20	4.392 − 5	1.091 − 3	2.648 − 4

z (km)	$\bar{T}$ (i = 9)	$\bar{T}$ (i = 10)	$\bar{T}$ (i = 11)
120	9.999 − 1	9.998 − 1	9.997 − 1
115	9.998 − 1	9.997 − 1	9.994 − 1
110	9.997 − 1	9.994 − 1	9.989 − 1
105	9.994 − 1	9.987 − 1	9.974 − 1
100	9.986 − 1	9.968 − 1	9.933 − 1
95	9.964 − 1	9.918 − 1	9.829 − 1
90	9.909 − 1	9.803 − 1	9.597 − 1
85	9.786 − 1	9.586 − 1	9.176 − 1
80	9.554 − 1	9.240 − 1	8.562 − 1
75	9.195 − 1	8.733 − 1	7.775 − 1
70	8.715 − 1	8.035 − 1	6.809 − 1
65	8.102 − 1	7.115 − 1	5.635 − 1
60	7.313 − 1	5.947 − 1	4.252 − 1
55	6.296 − 1	4.496 − 1	2.739 − 1
50	5.039 − 1	3.234 − 1	1.394 − 1
45	3.686 − 1	2.050 − 1	5.573 − 2
40	2.403 − 1	1.121 − 1	1.737 − 2
35	1.273 − 1	4.463 − 2	3.220 − 3
30	4.310 − 2	8.589 − 3	1.557 − 4
25	5.509 − 3	3.536 − 4	3.497 − 7
20	8.743 − 5	6.082 − 7	9.070 − 13

z (km)	$\bar{T}$ (i = 12)	$\bar{T}$ (i = 13)	$\bar{T}$ (i = 14)
120	9.994 − 1	9.982 − 1	9.979 − 1
115	9.989 − 1	9.967 − 1	9.962 − 1

TABLE A2. (*Continued*)

z (km)	$\bar{T}$ (i = 12)	$\bar{T}$ (i = 13)	$\bar{T}$ (i = 14)
110	9.977 − 1	9.934 − 1	9.920 − 1
105	9.947 − 1	9.849 − 1	9.808 − 1
100	9.868 − 1	9.654 − 1	9.533 − 1
95	9.675 − 1	9.291 − 1	8.993 − 1
90	9.293 − 1	8.753 − 1	8.165 − 1
85	8.713 − 1	8.043 − 1	7.117 − 1
80	7.985 − 1	7.145 − 1	5.907 − 1
75	7.091 − 1	6.053 − 1	4.561 − 1
70	5.998 − 1	4.781 − 1	3.152 − 1
65	4.717 − 1	3.404 − 1	1.818 − 1
60	3.327 − 1	2.095 − 1	7.879 − 2
55	1.998 − 1	1.028 − 1	2.182 − 2
50	9.627 − 2	3.446 − 2	2.880 − 3
45	3.567 − 2	6.752 − 3	1.354 − 4
40	9.359 − 3	6.498 − 4	1.525 − 6
35	1.158 − 3	1.615 − 5	9.508 − 10
30	2.323 − 5	1.684 − 8	8.491 − 16
25	8.472 − 9	1.387 − 14	5.186 − 28
20	4.906 − 16	1.801 − 27	0.0

z (km)	$\bar{T}$ (i = 15)	$\bar{T}$ (i = 16)	$\bar{T}$ (i = 17)
120	9.974 − 1	9.947 − 1	9.919 − 1
115	9.952 − 1	9.903 − 1	9.851 − 1
110	9.904 − 1	9.807 − 1	9.690 − 1
105	9.784 − 1	9.589 − 1	9.274 − 1
100	9.509 − 1	9.183 − 1	8.324 − 1
95	9.003 − 1	8.571 − 1	6.666 − 1
90	8.287 − 1	7.697 − 1	4.512 − 1
85	7.397 − 1	6.503 − 1	2.416 − 1
80	6.331 − 1	5.011 − 1	9.677 − 2
75	5.081 − 1	3.360 − 1	2.581 − 2
70	3.648 − 1	1.819 − 1	3.283 − 3
65	2.129 − 1	7.003 − 2	8.629 − 5
60	8.447 − 2	1.465 − 2	5.951 − 8
55	1.604 − 2	9.004 − 4	1.642 − 14
50	7.737 − 4	4.498 − 6	1.301 − 27
45	5.047 − 6	3.694 − 10	0.0
40	2.344 − 9	7.629 − 17	0.0
35	8.210 − 15	1.109 − 27	0.0
30	5.095 − 25	1.952 − 46	0.0
25	1.355 − 45	0.0	0.0
20	0.0	0.0	0.0

* Use O_2 column density N measured along the solar beam as the independent variable for interpolation purposes. The altitudes z correspond to the given N values for an overhead sun only.

** Read 3.922 + 16 as 3.922×10^{16}.

REFERENCES

Ackerman, M., 1971: Ultraviolet solar radiation related to mesospheric processes. *Mesospheric Models and Related Experiments*, G. Fiocco, Ed., D. Reidel, 149–159.

Anderson, J. G., 1971: Rocket-borne ultraviolet spectrometer measurement of OH resonance fluorescence with a diffusive transport model for mesospheric photochemistry. *J. Geophys. Res.*, **76**, 4634–4652.

Bates, D. R., and M. Nicolet, 1950: The photochemistry of atmospheric water vapor. *J. Geophys. Res.*, **55**, 301–327.

Bell, S., 1965: The spectra of H_2O and D_2O in the vacuum ultraviolet. *J. Mol. Spectros.*, **16**, 205–213.

Blake, A. J., 1979: An atmospheric absorption model for the Schumann-Runge bands of oxygen. *J. Geophys. Res.*, **84**, 3272–3282.

Bruecker, G. E., J. -D. F. Bartoe, O. Kjeldseth Moe and M. E. VanHoosier, 1976: Absolute ultraviolet intensities and their variations with solar activity. I. The wavelength region 1750–2100Å. *Astrophys. J.*, **209**, 935–944.

Bruner, E. C., Jr., and W. A. Rense, 1969: Rocket observations of profiles of solar ultraviolet emission lines. *Astrophys. J.*, **157**, 417–424.

Frederick, J. E., and R. D. Hudson, 1979: Predissociation line widths and oscillator strengths for the 2–0 to 13–0 Schumann-Runge bands of O_2. *J. Mol. Spectros.*, **74**, 247–256.

——, and ——, 1980: Dissociation of molecular oxygen in the Schumann-Runge bands. *J. Atmos. Sci.*, **37**, 1095–1102.

——, B. W. Guenther, P. B. Hays and D. F. Heath, 1978a: Ozone profiles and chemical loss rates in the tropical stratosphere deduced from backscatter ultraviolet measurements. *J. Geophys. Res.*, **83**, 953–958.

——, D. W. Rusch and S. C. Liu, 1978b: Nightglow emissions of $OH(X^2\pi)$: Comparison of theory and measurements in the (9–3) band. *J. Geophys. Res.*, **83**, 2441–2445.

Heroux, L., and R. A. Swirbalus, 1976: Full disk solar fluxes between 1230 and 1940 Å. *J. Geophys. Res.*, **81**, 436–440.

Herzberg, G., 1966: Molecular spectra and molecular structure III. *Electronic Spectra of Polyatomic Molecules*, D. Van Nostrand, 632 pp. (see pp. 194–201).

Hudson, R. D., 1971: Critical review of ultraviolet photoabsorption cross sections for molecules of astrophysical and aeronomic interest. *Rev. Geophys. Space Phys.*, **9**, 305–406.

——, and S. H. Mahle, 1972: Photodissociation rates of molecular oxygen in the mesosphere and lower thermosphere. *J. Geophys. Res.*, **77**, 2902–2914.

Hunt, B. G., 1966: Photochemistry of ozone in a moist atmosphere. *J. Geophys. Res.*, **71**, 1385–1398.

Kockarts, G., 1971: Penetration of solar radiation in the Schumann-Runge bands of molecular oxygen. *Mesospheric Models and Related Experiments*, G. Fiocco, Ed., D. Reidel, 160–176.

Krueger, A. J., and R. A. Minzner, 1976: A mid-latitude ozone model for the 1976 U.S. Standard Atmosphere. *J. Geophys. Res.*, **81**, 4477–4481.

McNesby, J. R., I. Tanaka and H. Okabe, 1962: Vacuum ultraviolet photochemistry III. Primary processes in the ultraviolet photolysis of water and ammonia. *J. Chem. Phys.*, **36**, 605–607.

Meier, R. R., and D. K. Prinz, 1970: Absorption of the solar Lyman alpha line by geocoronal atomic hydrogen. *J. Geophys. Res.*, **75**, 6969–6979.

Meinel, A. B., 1950: Hydroxide emission bands in the spectrum of the night sky. *Astrophys. J.*, **111**, 207–208.

Nicolet, M., 1975: Stratospheric ozone: An introduction to its study. *Rev. Geophys. Space Phys.*, **13**, 593–636.

Ogawa, M., 1968: Absorption coefficients of O_2 at the Lyman-alpha line and its vicinity. *J. Geophys. Res.*, **73**, 6759–6763.

Park, J. H., 1974: The equivalent mean absorption cross sections for the O_2 Schumann-Runge bands: Application of the H_2O and NO photodissociation rates. *J. Atmos. Sci.*, **31**, 1893–1897.

Riegler, J. R., S. K. Atreya, T. M. Donahue, S. C. Liu, B. Wasser and J. F. Drake, 1977: UV stellar occultation measurements of nighttime equatorial ozone. *Geophys. Res. Lett.*, **4**, 145–148.

Stief, L. J., W. A. Payne and B. Klemm, 1975: A flash photolysis-resonance fluorescence study of the formation of $O(^1D)$ in the photolysis of water and the reaction of $O(^1D)$ with H_2, Ar, and He. *J. Chem. Phys.* **62**, 4000–4008.

Streit, G. E., C. J. Howard, A. L. Schmeltekopf, J. A. Davidson and H. I. Schiff, 1976: Temperature dependence of $O(^1D)$

rate constants for reactions with O_2, N_2, CO_2, O_3, and H_2O. *J. Chem. Phys.*, **65**, 4761–4764.

Vidal-Madjar, A., J. E. Blamont and B. Phissamay, 1973: Solar Lyman alpha changes and related hydrogen density at the earth's exobase (1969–1970). *J. Geophys. Res.*, **78**, 1115–1144.

Watanabe, K., and M. Zelikoff, 1953: Absorption coefficients of water vapor in the vacuum ultraviolet. *J. Opt. Soc. Amer.*, **43**, 753–755.

Wofsy, S. C., 1978: Temporal and latitudinal variations of stratospheric trace gases: A critical comparison between theory and experiment. *J. Geophys. Res.*, **83**, 364–378.